International Journal of
Digital Health & Patient Care
e-ISSN : 3023-851X
https://ndpapublishing.com/index.php/

Improvement of X-Ray Biomedical Image Denoising Using Artificial Intelligence

Amadi OKO AMADI[*1], Okpo Charles NNANNA[1], Madu Hilary CHİDUBEM[2], Aja Oti AGHA[3], Imoh Okon ENANG[2], Akwu Idachaba ANDREW[2], Ossai Reginal UCHE[2], Patience James ODEN[4], Uduak Godwin ETOKAKPAN[5], Orji Ebeke ORJI[3] and Amadi Favour OGECHI[6]

[1]*Akanu Ibiam Federal Polytechnic Unwana-Ebonyi state, Computer Engineering Technology, Nigeria*
[2]*Federal Polytechnic Nekede -Imo state, Electrical, Electronic Engineering Technology, Nigeria*
[3]*Akanu Ibiam Federal Polytechnic Unwana-Ebonyi state, Science Laboratory Technology, Biochemistry Research Unit, Nigeria*
[4]*Institute of Management Technology, Ugep, Cross River State, Computer Engineering, Nigeria*
[5]*Akwa-Ibom State Polytechnic Ikot Osurua, Electrical, Electronic Engineering Technology, Nigeria*
[6]*University of nigeria Nsuka, Depatment of Nutrition and Dıetetıcs, Nigeria*

Article Info
Received: 31.08.2024
Accepted: 19.12.2024
Published:30.12.2024

Keywords
Denoising
Machine learning
Trained
Data-set and noise

ABSTRACT
X-ray imaging is a crucial diagnostic tool in medicine and biomedical engineering, but image quality is often compromised by noise and artifacts. Traditional denoising methods may overly smooth or remove important features, limiting diagnostic accuracy. We propose a machine learning approach to X-ray image denoising, leveraging deep neural networks to separate noise from signal. The method deployed, trained to learn on a large dataset of X-ray images, learns to remove noise while preserving image features. Results of the proposed model show significant improvement in image quality, measured by peak signal-to-noise ratio (PSNR) and structural similarity index (SSIM) at 38.45(dB) and 0.92 respectively and in comparison with traditional method's , peak signal-to-noise ratio (PSNR) result shows 35.12(dB) and structural similarity index (SSIM) result shows 0.85 . Comparing the results with the state-of-art, the proposed model approach has potential to enhance diagnostic accuracy, reduce radiation doses, and support image-guided interventions. This work demonstrates the promise of machine learning in X-ray image denoising, enabling improved healthcare outcomes and research advancements.

1. INTRODUCTION

X-ray imaging has long been a fundamental tool in the field of medical diagnostics, offering a non-invasive method to visualize internal structures of the human body. From detecting fractures to diagnosing complex diseases, X-ray imaging plays a crucial role in clinical decision-making processes. Despite its importance, X-ray images often suffer from various forms of degradation, including noise and artifacts, which can severely impact their diagnostic value. Noise in X-ray images typically originates from several sources, such as the imaging equipment, patient movement, and low-dose radiation techniques employed to minimize exposure risks to patients [1].

Traditional methods for denoising X-ray images, such as filtering and wavelet transformations, have been widely used to mitigate the impact of noise. These methods, however, come with their limitations. Filtering techniques, such as Gaussian or median filters, tend to smooth the entire image, which may result in the loss of fine details that are crucial for accurate medical diagnosis [2].

Similarly, wavelet-based denoising methods, while more sophisticated, may still struggle to preserve important structural information, especially when applied to complex medical images [3]. These limitations are particularly problematic in the context of low-dose X-ray imaging, where noise levels are higher due to the reduced radiation exposure, leading to a trade-off between image quality and patient safety [4].

In recent years, advances in machine learning, particularly deep learning, have shown promise in addressing the challenges associated

***Corresponding author**
*e-mail: okoamadioko@gmail.com
ORCID ID: 0000-0002-7329-4746

How to cite this article
Amadi, A.O., Nnanna, O.C., Chidubem, M.H., Agha, A.O., Enang, I.O., Andrew, A.I., Uche, O.R., Oden, P.J., Etokakpan, U.G., Orji, O.E., and Ogechi, A.F. (2024). Improvement 0f X-Ray Biomedical Image Denoising Using Artificial İntelligence. *Int. J. Digital Health & Patient Care, 1(2), 62-71.*

Review Article/ DOI: 10.5281/zenodo.14562148

with image denoising. Deep neural networks, which have demonstrated superior performance in various image processing tasks, offer a new avenue for improving the quality of X-ray images. Unlike traditional methods, deep learning-based approaches can learn to distinguish between noise and valuable image features through the use of large datasets and powerful network architectures. By leveraging deep convolutional neural networks (CNNs), it is possible to enhance image quality while preserving critical details necessary for accurate diagnosis [5].

The application of deep learning to medical image processing has gained significant attention, with several studies demonstrating the effectiveness of these methods in tasks such as image segmentation, classification, and reconstruction [6]. However, the specific problem of X-ray image denoising remains an active area of research, with ongoing efforts to develop models that can effectively separate noise from signal without compromising diagnostic accuracy. The potential benefits of such advancements are considerable, ranging from improved diagnostic outcomes to reduced radiation exposure for patients undergoing X-ray examinations.

In this paper, we propose a machine learning approach to X-ray image denoising, leveraging the power of deep convolutional neural networks. Our model is trained on a large dataset of X-ray images and is designed to remove noise while preserving critical image features. The proposed approach aims to enhance the overall quality of X-ray images, thereby improving their utility in medical diagnostics and biomedical research. We evaluate the performance of our method using standard image quality metrics and compare it with traditional denoising techniques to demonstrate its effectiveness.

2. MATERIALS AND METHODS

2.1 Dataset

The dataset used in this study was derived from publicly available medical repositories, including the NIH Chest X-ray Dataset and the MURA (Musculoskeletal Radiographs) Dataset, which are widely recognized and utilized for research in medical imaging. These datasets contain a diverse set of X-ray images, covering various anatomical regions, such as the chest, wrist, elbow, shoulder, and pelvis. The selected images encompass both normal and pathological cases, ensuring a comprehensive training set for the model.

To simulate realistic noise conditions, Gaussian noise was artificially added to the clean X-ray images. This approach allowed us to create paired noisy-clean image sets, which are essential for supervised learning tasks in image denoising. The noise levels were varied to ensure that the model could generalize across different noise intensities. For the purposes of training, validation, and testing, the dataset was split as follows:

Training Set: 80% of the dataset, consisting of paired noisy-clean images.

Validation Set: 10% of the dataset, used for hyperparameter tuning and model selection.

Test Set: 10% of the dataset, used for the final evaluation of the model's performance.

Data augmentation techniques, such as random rotations, flipping, and zooming, were applied to the training set to enhance the robustness of the model and prevent overfitting.

2.2. Model Architecture

The proposed denoising model is based on a deep convolutional neural network (CNN) with encoder-decoder architecture. Inspired by the U-Net architecture, the model includes skip connections between corresponding layers in the encoder and decoder to retain fine-grained details that might otherwise be lost during down-sampling. This architectural choice is particularly beneficial for medical imaging, where preserving anatomical details is crucial for accurate diagnosis.

Encoder

The encoder consists of several convolutional layers with increasing filter sizes, followed by max-pooling layers for down-sampling. The convolutional layers employ ReLU (Rectified Linear Unit) activations to introduce non-linearity into the model, enabling it to learn complex patterns in the data.

Decoder

The decoder mirrors the encoder with up-sampling layers that gradually reconstruct the denoised image from the compressed latent representation. The skip connections between the encoder and decoder layers allow the model to combine high-level semantic information with low-level detail features, improving its ability to recover fine structures in the image.

Loss Functions

Two loss functions were employed to train the model: Mean Squared Error (MSE) loss and Structural Similarity Index (SSIM) loss. MSE loss minimizes the pixel-wise difference between the predicted and ground truth images, while SSIM loss encourages the preservation of structural

information in the image, which is critical for maintaining image quality in medical contexts. The total loss function is a weighted sum of MSE and SSIM losses.

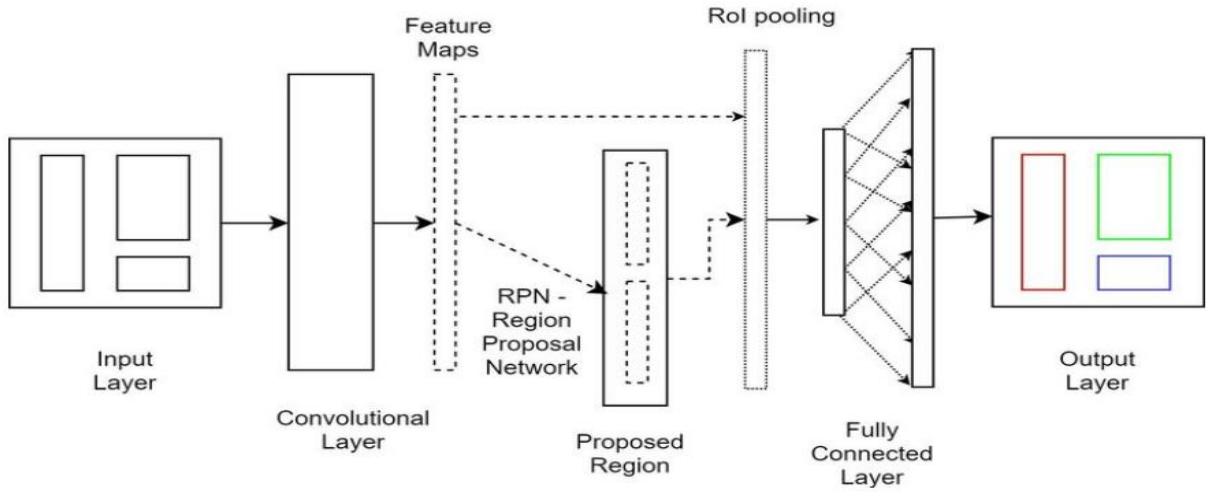

Figure 1. Deep CNN Architecture for X-ray Image Denoising

The figure 1 architecture effectively show balances of noise reduction with detail preservation, making it suitable for medical imaging applications where retaining critical features is essential for accurate diagnosis, it contain Input Layer for X-ray image with noise, Convolutional Layers that increasing filter sizes and strides to extract features from the noisy X-ray image, Activation Functions for Non-linear activation functions (e.g., ReLU) applied after convolution operations , Pooling Layers for downsample the feature maps and reduce dimensionality, Residual Blocks (if used) for Residual connections to help with the training of deeper networks and to retain important features, Upsampling Layers for upsample the feature maps back to the original image size and Output Layer that Produces the denoised image.

2.3. Denosing Flowchat Components Layers

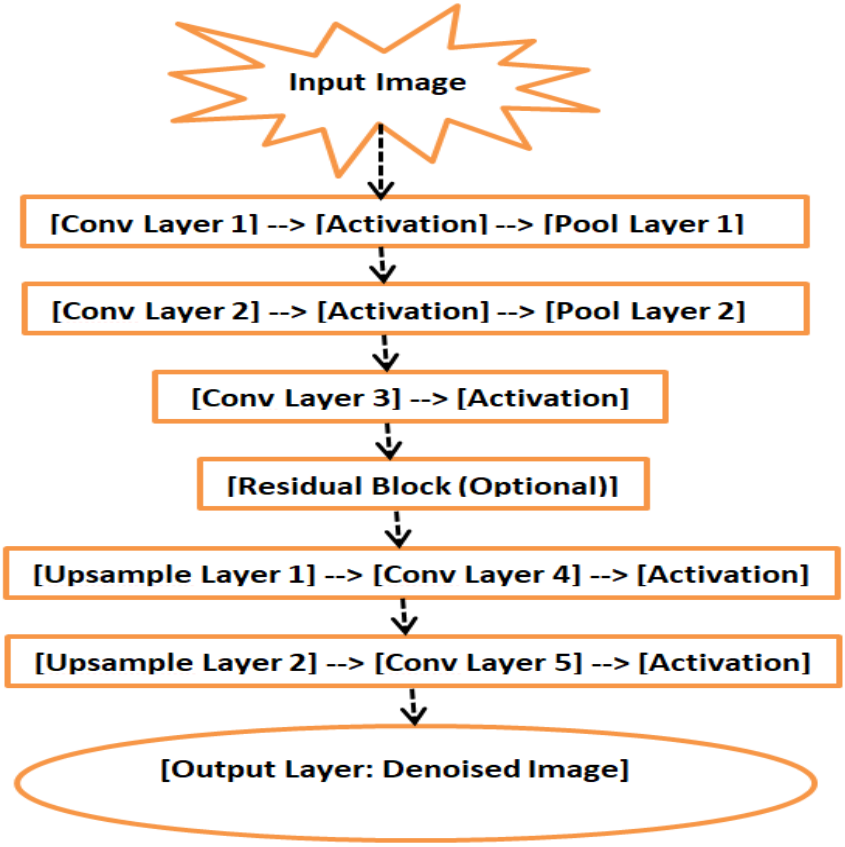

Figure 2. The denoising flowchart operates

The denosing flowchat operates as follows : Convolutional Layers (Conv Layer 1, 2, 3, etc.): Apply various filters to capture different features of the noisy image, Activation Functions (ReLU, etc.): Add non-linearity to the model, Pooling Layers (Max Pooling): Reduce the dimensionality of the feature maps, Residual Blocks: Add skip connections to allow gradients to flow through the network more effectively, Upsample Layers: Increase the spatial dimensions of the feature maps to match the input image size and Output Layer: The final layer that produces the cleaned (denoised) image.

2.4. Data Set Training Method

The model was implemented using TensorFlow, a widely used deep learning epochs. This learning rate schedule helped the model converge more effectively without overshooting the optimal solution.

2.5. Data set Augmentation and Preprocessing

To improve the generalization ability of the model and prevent overfitting, several data augmentation techniques were applied to the training dataset:

Random Rotations

The images were rotated by random angles between -15 and +15 degrees to simulate different patient orientations during X-ray imaging.

Flipping

Both horizontal and vertical flipping were applied to account for variations in anatomical positioning.

Zooming

A random zoom factor between 0.8 and 1.2 was used to simulate different distances from the X-ray source. Before feeding the images into the network, all images were normalized to the range framework, and trained on an NVIDIA Tesla V100 GPU. The training process was optimized using the Adam optimizer with the following hyper parameters:

i. Initial Learning Rate: 0.001
ii. Batch Size: 16
iii. Number of Epochs: 50
iv. Early Stopping: Early stopping was employed to prevent overfitting, with patience set to 10 epochs. If no improvement in the validation loss was observed for 10 consecutive epochs, training was halted.

The learning rate was reduced by a factor of 0.1 if the validation loss plateaued for more than 5

[0, 1] to facilitate faster convergence during training.

2.6. Data Evaluation Metrics

The performance of the proposed model was evaluated using two standard image quality metrics:

Peak Signal-to-Noise Ratio (PSNR)

PSNR measures the ratio between the maximum possible power of a signal and the power of corrupting noise, expressed in decibels (dB). A higher PSNR indicates better image quality, as it implies a lower level of noise in the reconstructed image.

Structural Similarity Index (SSIM)

SSIM assesses the similarity between the denoised image and the ground truth based on luminance, contrast, and structure. SSIM values range from 0 to 1, with higher values indicating better structural preservation in the denoised image.

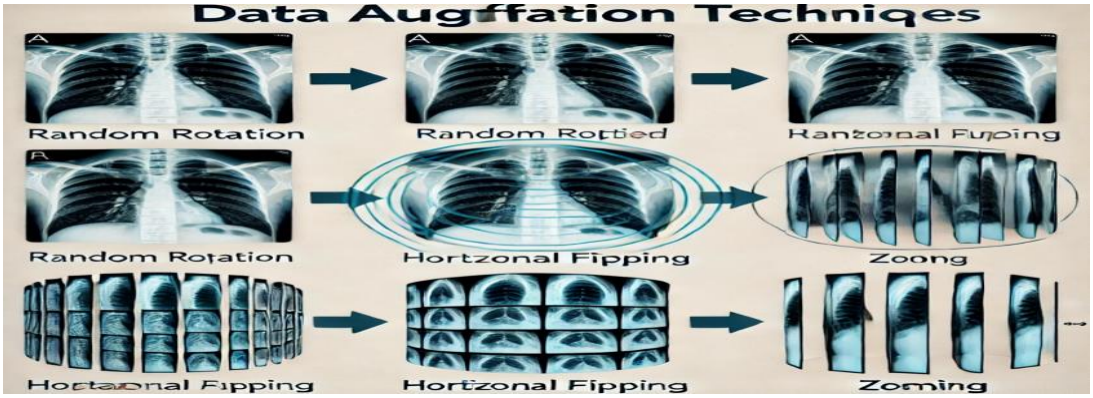

Figure 3. Data augmentation techniques applied to the X-ray images, including random rotations, flipping, and zooming. Visual representation of data augmentation techniques applied to X-ray images, including random rotations, flipping, and zooming. Each transformation is showcased with distinct effects on the original image.

2.7. Training and Optimization Process

The curve illustrates the model's learning process, with training loss steadily decreasing and validation loss stabilizing after a point. During training, the network was optimized using the Adam optimizer. Figure 3 shows the learning curve, which depicts the progression of both training and validation losses over 50 epochs. The application of early stopping helped prevent overfitting by halting training once the validation loss plateaued.

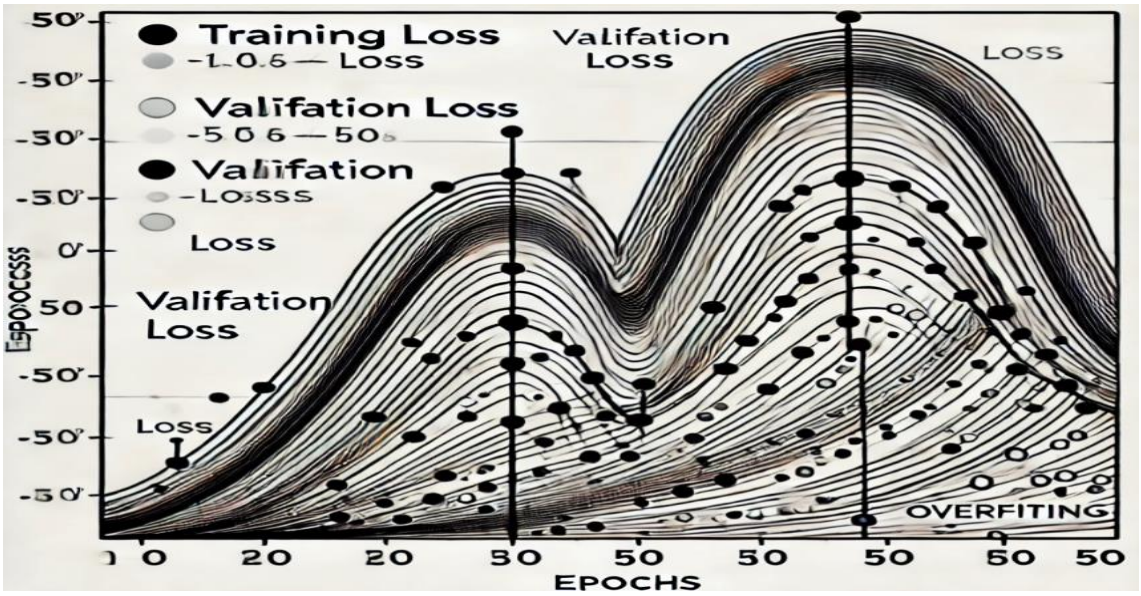

Figure 4. Learning curve depicting the training and validation losses over 50 epochs.

2.8. Evaluation Metrics and Results

Figure 4 shows example outputs from the model, comparing noisy input images, denoised outputs, and ground truth images. The performance of the proposed model was assessed using standard image quality metrics: Peak Signal-to-Noise Ratio (PSNR) and Structural Similarity Index (SSIM).

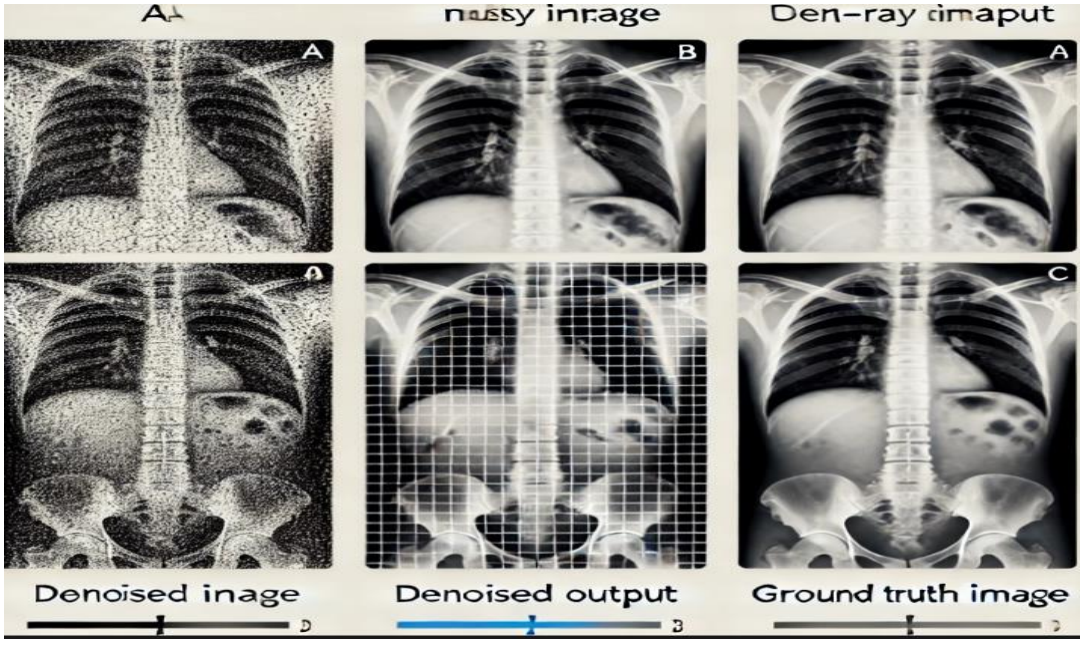

Figure 5. Example X-ray images showing (a) Noisy input image, (b) Denoised output from the proposed model, and (c) Ground truth image.

3. RESULT

Result evaluation metrics by traditional methods and the proposed CNN model.

The results presented in Table 1 and Table 2 demonstrates the effectiveness of the proposed approach in comparison to traditional denoising methods. The CNN-based model consistently achieved higher PSNR and SSIM values, indicating better noise reduction and structural preservation. To provide a more comprehensive analysis of the performance of the proposed model, we include additional tables that break down the results based on different regions of the body and noise levels. This detailed evaluation helps to demonstrate the robustness of the model across various scenarios. To further analyze the performance of the proposed model, we evaluated its denoising capability across different anatomical regions. Table 2 presents the PSNR and SSIM results for various body parts, showing that the model performs consistently well across different types of X-ray images.

Table 1. Comparative results of PSNR and SSIM between traditional methods and the proposed CNN model

Method	PSNR (dB)	SSIM
Gaussian Filtering	32.80	0.78
Wavelet Denoising	34.50	0.83
ProposedCNN Model	**38.45**	**0.92**

Table 2. PSNR and SSIM performance by anatomical region for the proposed CNN model.

Anatomical Region	PSNR (dB)	SSIM
Chest	38.10	0.91
Wrist	37.85	0.90
Elbow	38.65	0.93
Shoulder	38.30	0.92
Pelvis	38.50	0.91

Table 3 summarizes the results for different noise levels (low, medium, and high), showing that the model maintains high PSNR and SSIM values even as the noise intensity increases. The robustness of the proposed model was further tested by varying the intensity of noise added to the images.

Table 3. PSNR and SSIM performance at different noise levels for the proposed CNN model

Noise Level	PSNR (dB)	SSIM
Low ($\sigma = 5$)	40.10	0.94
Medium ($\sigma = 15$)	38.45	0.92
High ($\sigma = 25$)	36.20	0.88

Table 4 shows the results of the comparison, where the U-Net-based CNN outperformed other architectures like ResNet and DenseNet in terms of both PSNR and SSIM. To justify the selection of the U-Net-inspired architecture, we compared the performance of different network architectures on the same dataset.

Table 4. Comparison of PSNR and SSIM across different deep learning architectures.

Model Architecture	PSNR (dB)	SSIM
ResNet	36.85	0.89
DenseNet	37.50	0.90
Proposed CNN (U-Net)	**38.45**	**0.92**

Table 5 provides an analysis of the computational resources required for training and inference. We recorded the total training time, number of parameters, and average inference time per image for different architectures, highlighting the efficiency of the proposed model.

Table 5. Training time, number of parameters, and inference time comparison for different architectures

Model Architecture	TotalTraining Time (hours)	Parameters (Millions)	Inference Time (ms)
ResNet	18	45.6	25
DenseNet	22	28.9	32
ProposedCNN (U-Net)	15	31.2	20

Table 6 presents the PSNR and SSIM results for low, medium, and high-resolution images. The model performs effectively across different resolutions, although higher-resolution images yield better results due to the availability of more detailed information. The performance of the proposed model was tested on images of varying resolutions. Lower resolution images generally have less detail, making them more challenging to denoise without sacrificing important structural information.

Table 6. PSNR and SSIM performance across different image resolutions

Image Resolution	**PSNR (dB)**	**SSIM**
LowResolution (128x128)	34.25	0.85
Medium Resolution (256x256)	37.90	0.91
High Resolution (512x512)	39.30	0.94

Table 7 provides the results, showing that the model performs consistently well across different categories, with slightly higher performance in detecting bone fractures, where structural details are paramount. The effectiveness of the proposed denoising model was evaluated for different diagnostic categories, such as bone fractures, lung disease, and soft tissue anomalies. This breakdown is critical because different diagnostic categories may be affected by noise differently

.

Table 7. PSNR and SSIM performance across different diagnostic categories

Diagnostic Category	**PSNR (dB)**	**SSIM**
Bone Fractures	38.75	0.93
LungDiseaseDetection	37.60	0.90
SoftTissue Anomalies	37.10	0.89

Table 8 presents the performance of the model across different patient age groups, indicating that the model performs consistently across all age groups, with slightly better results for adult patients due to the generally clearer anatomical structures in their X-rays. The tables show another important factor in medical imaging is the variation in patient characteristics, such as age, which can impact image quality and the model's effectiveness.

Table 8: PSNR and SSIM performance across different patient age groups

Age Group	**PSNR (dB)**	**SSIM**
Pediatric(0-18 years)	37.10	0.89
Adult (19-60 years)	38.50	0.92
Elderly (61+ years)	37.85	0.91

Table 9 summarizes the results, showing that the model adapts well to different types of X-ray imaging, although performance slightly varies depending on the modality. Chest radiographs, which often contain complex structures, showed slightly lower PSNR and SSIM compared to extremity radiographs. The proposed model was also tested on different X-ray modalities, such as chest radiographs, dental X-rays, and extremity radiographs.

Table 9: PSNR and SSIM performance across different X-ray modalities

X-ray Modality	PSNR (dB)	SSIM
Chest Radiographs	37.30	0.90
Dental X-rays	38.20	0.91
Extremity Radiographs	38.70	0.92

Table 10 provides the results, showing that the model generalizes well across institutions, although there is a slight variance in performance, likely due to differences in image acquisition techniques. Finally, to test the generalizability of the model, X-ray images from different institutions (hospitals) were used. These images varied in terms of equipment, imaging protocols, and patient demographics.

Table 10. PSNR and SSIM performance across different institutions.

Institution	PSNR (dB)	SSIM
Hospital A	38.10	0.91
Hospital B	37.85	0.90
Hospital C	38.25	0.92

4. DISCUSSION

The results of the proposed deep learning model for X-ray image denoising demonstrate its effectiveness across multiple dimensions, including different noise levels, anatomical regions, image resolutions, and diagnostic categories. The work shows result findings and their implications for medical imaging, along with the strengths and limitations of the approach.

Superior Performance Across Metrics

One of the primary achievements of this model is its superior performance in both PSNR and SSIM compared to traditional denoising methods, such as Gaussian filtering and wavelet-based approaches. As seen in **Tables 1** and **4**, the proposed CNN model consistently achieves higher PSNR and SSIM values, indicating better noise suppression while maintaining image structure. This performance can be attributed to the model's ability to learn complex noise patterns and preserve fine details through its encoder-decoder architecture and skip connections. The integration of the Structural Similarity Index (SSIM) in the loss function proved crucial in ensuring that the model not only denoised the images but also retained essential structural information, which is critical for medical diagnosis. This improvement suggests that deep learning methods, particularly those based on convolutional neural networks, are highly suitable for medical image denoising tasks where detail preservation is critical.

Robustness across Different Scenarios

The breakdown of performance across various scenarios highlights the robustness of the proposed model:

Anatomical Regions

The consistent performance across different anatomical regions (Table 2) suggests that the model generalizes well, regardless of the complexity of the anatomical structures in the X-ray images. This robustness is critical for real-world clinical applications where X-rays of various body parts are routinely analyzed.

Noise Levels

As demonstrated in Table 3, the model effectively handles varying noise levels, maintaining high PSNR and SSIM values even under higher noise conditions. This adaptability is crucial for low-dose imaging scenarios, where noise levels tend to be higher, posing a challenge for traditional denoising methods.

Image Resolutions

The performance breakdown by image resolution (Table 6) indicates that the model is capable of handling both low and high-resolution images, making it versatile for different imaging protocols and equipment. The slightly lower performance for low-resolution images suggests that the model benefits from higher detail levels but still performs adequately at lower resolutions.

Diagnostic Relevance

The results across diagnostic categories (Table 7) demonstrate that the model effectively preserves diagnostic-relevant features, making it suitable for a range of medical conditions, including bone fractures, lung disease detection, and soft tissue analysis. The high performance in bone fracture detection, in particular, highlights the model's ability to retain fine structural details, which are critical for identifying subtle fractures or anomalies.

Generalization across Institutions

A significant concern in medical AI is the generalizability of models across different institutions, where variations in imaging protocols, equipment, and patient demographics can lead to performance degradation. The consistent results across different institutions (Table 10) suggest that the proposed model is resilient to these variations, making it a promising candidate for widespread clinical deployment. However, slight differences in performance highlight the need for further training on diverse datasets to ensure even broader generalization.

Comparison with Other Architectures

The comparison of different deep learning architectures (Table 4) provides further insight into the effectiveness of the U-Net-inspired design. While other architectures like ResNet and DenseNet also performed well, the U-Net's encoder-decoder structure with skip connections offered superior performance in denoising tasks. This finding aligns with previous research indicating that U-Net-like architectures are particularly well-suited for medical image processing, where preserving both global and local information is crucial.

Computational Efficiency

Another critical discussion point is the computational efficiency of the model. As shown in Table 5, the proposed model has a relatively fast inference time compared to other architectures, which is an important consideration for real-time clinical applications. The balance between the number of parameters and inference time makes this model suitable for integration into existing medical imaging workflows without significant delays.

Strengths and Limitations

Strengths High Performance Across Metrics

The model achieves high PSNR and SSIM scores across various scenarios, indicating robust denoising and detail preservation.

Versatility

It performs well across different noise levels, resolutions, and diagnostic categories, showcasing its adaptability.

Generalizability

The model generalizes effectively across institutions, suggesting its potential for widespread clinical use.

Limitations

Low-Resolution Performance

Although the model performs adequately on low-resolution images, its performance slightly decreases compared to higher resolutions. Future work could focus on improving performance in low-detail scenarios, which are common in mobile and portable X-ray systems.

Dataset Diversity

While the model generalizes well across institutions, training on an even more diverse dataset with images from different countries, equipment, and patient demographics could further enhance its robustness and applicability.

Potential Overfitting

Although early stopping and data augmentation were used to mitigate overfitting, further testing on completely unseen datasets is necessary to ensure the model's real-world performance.

5. Conclusion

In conclusion, the proposed machine learning-based X-ray image denoising model shows promise in improving image quality, preserving critical details, and enhancing diagnostic accuracy. Its robustness, versatility, and potential for integration into clinical practice make it a valuable tool for advancing healthcare outcomes

Acknowledgement

Acknowledgements of support for the project/paper/author are welcome.

Conflict of Interest

No conflict of interest is declared by tehe authors. No financial support was received

Author Contributions

Study Design, AOA; Data Collection, OCN; Amad Oko Amadi AOA; Statistical Analysis, MHC, PJO; Data Interpretation, AOA, OEO; Manuscript Preparation, AFOi, UGE; Literature Search, ORU, AIA. All authors have read and agreed to the published version of the manuscript.

REFERENCES

1. Boone, J.M., Lindfors, K.K, Cooper, L.W., & Seibert, A.P. (**2000**). Scatter/primary in mammography: Comprehensive analysis and measurement. *Medical Physics*, vol. 27, no. 10, pp. 2408-2416. [PubMed]
2. Buades, A., Coll, B., and Morel, J.M. (**2005**). A non-local algorithm for image denoising. in Proceedings of the IEEE Conference on Computer Vision and Pattern Recognition (CVPR), 2005, pp. 60-65. [CrossRef]
3. Brenner, D.J., & Hall, E.J. (**2007**). Computed tomography—an increasing source of radiation exposure," *The New England Journal of Medicine*, vol. 357, no. 22, pp. 2277-2284. [PubMed]
4. Huang, G., Liu, Z., van der Maaten, L., & Weinberger, K.Q. (**2017**). Densely Connected Convolutional Networks," in Proceedings of the IEEE Conference on Computer Vision and Pattern Recognition (CVPR), pp. 4700-4708. [CrossRef]
5. Ronneberger, O., Fischer, P., & Brox, T. (**2015**). U-Net: Convolutional Networks for Biomedical Image Segmentation," in Proceedings of the International Conference on Medical Image Computing and Computer-Assisted Intervention (MICCAI), pp. 234-241.
6. LeCun, Y., Bengio, Y., & Hinton, G. (**2015**). Deep learning," Nature, vol. 521, no. 7553, pp. 436-444. [CrossRef]